Energy 281 (2023) 128158

Contents lists available at ScienceDirect

Energy

journal homepage: www.elsevier.com/locate/energy

# Multi-objective optimisation of a power generation system integrating solid oxide fuel cell and recuperated supercritical carbon dioxide cycle

Dibyendu Roy, Samiran Samanta, Sumit Roy *, Andrew Smallbone, Anthony Paul Roskilly

*Department of Engineering, Durham University, Durham, DH1 3LE, UK*

ARTICLE INFO

Handling Editor: A. Olabi

*Keywords:*
Response surface methodology
SOFC
Supercritical $CO_2$ cycle
Hydrogen
Multi-objective optimisation
Waste heat recovery

ABSTRACT

This article presents an advanced power generation system that integrates a solid oxide fuel cell (SOFC) module with a recuperated supercritical $CO_2$ (s-$CO_2$) cycle. The waste heat generated by the exhaust of the SOFC module is utilised to drive the s-$CO_2$ cycle, resulting in enhanced energy efficiency. The performance of the system was investigated through thermodynamic and economic analyses and optimised using response surface methodology. The optimisation process focused on two objectives: maximising the energy efficiency of the integrated system and minimising the levelised cost of electricity. The study meticulously analysed the effects of important variables such as current density, fuel utilisation factor, and operating temperature of the fuel cell. The optimisation efforts yielded impressive results, achieving an energy efficiency of 64% and a levelised cost of electricity (LCOE) of 0.18£/kWh. The proposed system surpassed traditional natural gas-fuelled power plants in terms of efficiency and specific emissions. Furthermore, the system's performance was evaluated when operated with green hydrogen fuel, which led to a substantial improvement in efficiency, estimated at 73.37%. However, it was found that the LCOE of the system is relatively higher and approximately 15% higher than the methane-based alternative.

## 1. Introduction

It is projected that fossil fuels currently account for 80% or more of the world's primary energy consumption [1]. This heavy reliance on fossil fuels results in significant greenhouse gas emissions, endangering the International Panel on Climate Change's recommendation of limiting global warming to below 2° Celsius [2]. This has raised the alarm about the need to reduce the amount of carbon dioxide ($CO_2$) in the atmosphere. As a result, governments are shifting toward an economy based on renewable energy.

In recent years, considerable emphasis has been placed on developing fuel cell-based energy systems, since fuel cells are thought to be superior to other traditional energy devices in terms of reaching sustainable energy goals. Fuel cells can be classified into different categories based on their operating temperature. The solid oxide fuel cell (SOFC) and molten carbonate fuel cells, which operate at temperatures exceeding 600 °C, are examples of high-temperature fuel cells [3]. SOFCs are commonly used in stationary power generation due to their higher efficiency. Their high operating temperatures make them suitable for direct internal reforming, allowing the use of biogas, methane, or other higher hydrocarbon fuels as energy sources.

In contrast, low-temperature fuel cells such as polymer electrolyte membrane fuel cells (PEMFCs) are less expensive than SOFCs. The higher cost of SOFCs can be attributed primarily to their lower production quantities [4,5]. However, due to their high operating temperatures and the generation of high-grade waste heat, SOFCs are well-suited for integration with bottoming cycles, which further utilise the waste heat to improve the overall system efficiency. This advantage makes SOFCs more advantageous compared to PEMFCs.

The integration of SOFCs into energy systems has been extensively studied. For example, Pirkandi et al. [6] investigated SOFC and gas turbine (GT) systems by connecting two SOFC stacks in series and parallel, respectively. Their study revealed that a hybrid system with two fuel cell stacks in sequence achieved a maximum electrical efficiency of 46.3%. Kumar et al. [7] performed a thermodynamic analysis of a comprehensive system that incorporated SOFCs, GTs, and an organic Rankine cycle (ORC), demonstrating that the energy and exergy efficiencies could reach up to 47.34% and 56.85%, respectively. Lei et al. [8] conducted a thermo-economic analysis of a SOFC-GT-ORC combined plant, comparing various working fluids in the ORC. Wang et al. [9] also investigated a similar SOFC-GT-ORC system using thermodynamic and

* Corresponding author.
*E-mail address:* sumit.roy@durham.ac.uk (S. Roy).

https://doi.org/10.1016/j.energy.2023.128158
Received 17 February 2023; Received in revised form 12 June 2023; Accepted 15 June 2023
Available online 25 June 2023

**Nomenclature**

| | |
|---|---|
| $\dot{a}_r$ | Extent of steam reforming reaction for $CH_4$, mol/s |
| $A_{cell}$ | Area of a cell, $m^2$ |
| AB | Afterburner |
| AHE | air heat exchanger |
| ANOVA | Analysis of variance |
| $\dot{b}_r$ | Extent of water gas shift reaction, mol/s |
| $\dot{c}_r$ | Extent of electrochemical reaction, mol/s |
| CAPEX | Capital cost, £ |
| $D_{Anode,eff}$ | Effective gaseous diffusivity through anode, $m^2/s$ |
| $D_{Cathode,eff}$ | Effective gaseous diffusivity through cathode, $m^2/s$ |
| DOE | Design of experiments |
| F | Faraday constant, C/mol |
| FHE | Fuel heat exchanger |
| h | Specific enthalpy, kJ/kg |
| j | Current density, $A/m^2$ |
| $j_{AS}$ | Limiting current density of anode, $A/m^2$ |
| $j_{CS}$ | Limiting current density of cathode, $A/m^2$ |
| $j_{OA}$ | Exchange current density of anode, $A/m^2$ |
| $j_{OC}$ | Exchange current density of cathode, $A/m^2$ |
| K | Equilibrium constant |
| L | Thickness, m |
| LCOE | Levelised cost of energy, £/kWh |
| $LHV_{fuel}$ | Lower heating value, kJ/kg |
| $\dot{m}$ | Mass flow rate, kg/s |
| $\dot{n}$ | Molar flow rate, mol/s |
| $\overline{R}$ | Universal gas constant, J/mol.K |
| RSM | Response surface methodology |
| $\overline{s}$ | Molar entropy, J/mol·K |
| T | Operating temperature of SOFC |
| UF | Fuel utilisation factor |
| V | Voltage, V |
| $\dot{W}$ | Power, kW |
| WHE | Water heat exchanger |
| $Z_{CAP_i}$ | Investment cost for ith component, £ |

*Greek letters*

| | |
|---|---|
| η | Efficiency, % |
| ρ | resistivity of cell components |

*Subscripts*

| | |
|---|---|
| *act* | Activation |
| An | Anode |
| BA | Air blower |
| Ca | Cathode |
| IN | Inlet |
| FC | Fuel compressor |
| OUT | Outlet |
| SCC | $CO_2$ compressor |
| SCT | $CO_2$ turbine |

economic analyses. A homogeneous charge compression ignition (HCCI) engine was integrated with SOFC by Kim et al. [10] and further experimentally validated the proof of concept by Koo et al. [11]. Their experimental study demonstrated that about 75.1% of the waste heat was recovered. Additionally, multi-objective analysis of SOFC integrated combined heat and power system was explored by Mojaver et al. [12] using Taguchi approach and multi-criteria decision making (MCDM) method. According to their study, current density was found to be most effective parameter on power generation (71.5%).

The supercritical $CO_2$ cycle can be effectively used using high and medium temperature waste heat because of its simpler configuration, compactness, and relative high efficiency [13]. $CO_2$ is non-corrosive, non-flammable, non-toxic, and readily available. Furthermore, because the critical temperature of $CO_2$ is close to that of the atmosphere (31.1 °C), reaching a supercritical state is easily thermally feasible [14] and investment cost of s-$CO_2$ cycle is lower [15]. In order to recover waste heat from engine exhaust, Sakalis et al. [16] investigated the combination of the s-$CO_2$ cycle with a ship engine. Chen et al. [17] performed a techno-economic analysis of an integrated system combination of biomass gasification based GT cycle, s-$CO_2$ cycle, and coal fired system. The net present value of the system was calculated to be k $31358.34. Guo et al. [18] performed a systematic review of the s-$CO_2$ cycle related to technological advancement, key issues, and potential application in the energy sector.

Response surface methodology (RSM) is an effective method for performing multi-objective optimisation. Earlier, it was employed to optimise the performance of reactive cotton dying process [19], gasifier design [20], diesel engine using blends of Solketal, biodiesel and diesel [21], free piston Stirling engine [22], biogas setup for household energy applications [23], supercritical $CO_2$ extraction [24], external roller burnishing operation using a CNC lathe [25], conversion of tomato pomace into bio-oil [26], to increase the efficiency of the secondary flow injection from the axial gas turbine casing [27], stand-alone operation of vertical cylindrical thermal energy storage tank [28]. However, RSM is applied in very few studies related to integrated energy systems. Pourali and Esfahani [29] investigated an integrated hydrogen production system and optimised the performance using RSM. Mojaver et al. [30] investigated an integrated biomass gasification, SOFC and high temperature sodium heat pipe system using RSM. This demonstrates the effectiveness of RSM as a highly accurate multi-objective optimisation method.

Despite the potential of integrating SOFCs and recuperated s-$CO_2$ cycle systems in achieving sustainable energy goals, previous research on this specific configuration has been limited. In this study, we employ RSM to investigate the integrated SOFC and recuperated s-$CO_2$ cycle system. The system is modelled using methane-fuelled SOFC and integrated as a bottoming cycle with the s-$CO_2$ cycle. The objective of this study is to determine the optimal operating parameters of the integrated system and evaluate its performance and efficiency through comprehensive thermodynamic and economic analyses. Multi-objective optimisation is employed to determine the ideal operating conditions. Additionally, we slightly modify the proposed SOFC-s-$CO_2$ configuration to accommodate green hydrogen as a fuel and investigate the system's performance. This first-of-its-kind study provides valuable insights for future research on integrated energy systems and contributes to the advancement of sustainable energy solutions.

## 2. Materials and methods

### 2.1. System description

Fig. 1 depicts the detailed schematic of the proposed integrated energy system, showcasing the various components and their interconnections. At the heart of the system is the solid oxide fuel cell (SOFC), serving as the prime mover. The SOFC operates using methane as its fuel source, which undergoes a series of processes to enable efficient power generation. The methane fuel, after being compressed and heated, enters the system through a fuel heat exchanger (FHE) where it is further prepared. Simultaneously, fresh water is supplied to the system via a pump and passes through a water heat exchanger (WHE) to optimise its temperature for subsequent use. Inside the SOFC's anode channel, the steam-to-fuel ratio is maintained at 2.5 to ensure optimal

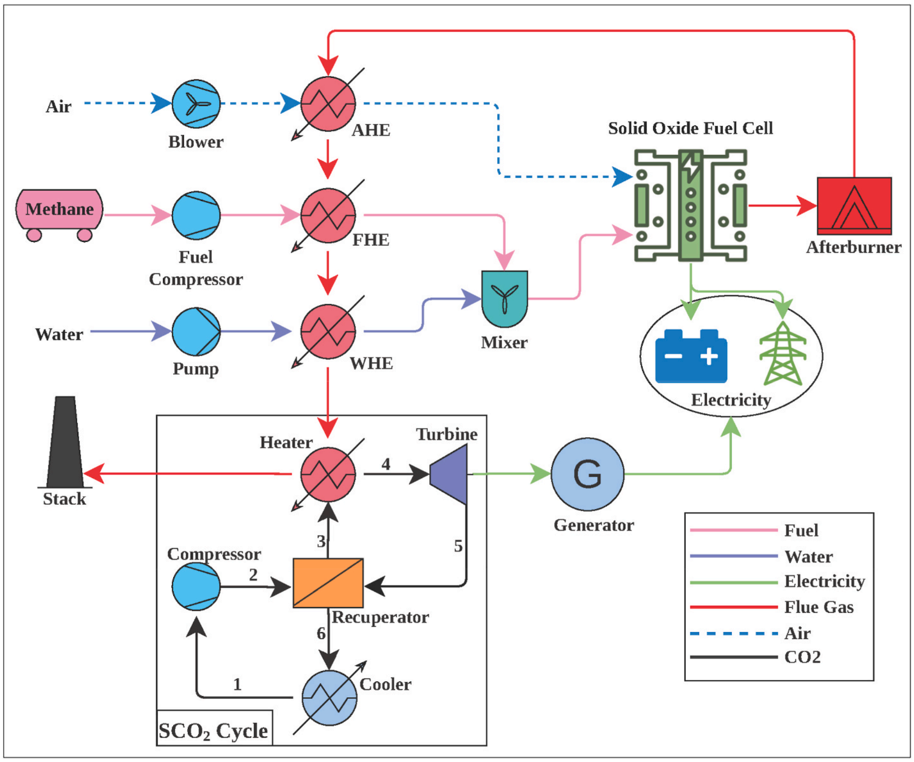


**Fig. 1.** Schematic diagram of the proposed system.

performance. The fuel and steam mixture undergoes electrochemical reactions within the SOFC, generating power as a result. To support the SOFC's operation, fresh air is drawn in and compressed by an air compressor. The compressed air is then heated in an air heat exchanger (AHE) to the appropriate temperature before being supplied to the cathode channel of the SOFC. This controlled airflow facilitates the electrochemical reactions necessary for power generation within the fuel cell. In the SOFC's anode channel, any unused fuel exiting the channel is directed to the afterburner (AB) unit. In the afterburner, the remaining fuel is entirely consumed, ensuring complete utilisation. The heat generated from the afterburner's exhaust gas is efficiently harnessed to further elevate the temperature of the incoming streams within the SOFC, maximising the overall energy efficiency of the system. In addition to the SOFC module, the integrated energy system incorporates a recuperated supercritical $CO_2$ cycle. This cycle takes advantage of the waste heat produced by the gas heater, utilising it as the driving force for the supercritical $CO_2$ cycle. The waste heat is effectively recovered and converted into useful energy, contributing to the system's overall performance and efficiency. By integrating these various components and optimising their operation, the proposed integrated energy system demonstrates a highly efficient and sustainable approach to power generation.

### 2.2. Solid oxide fuel cell

The SOFC model investigated in this study is of the internal reforming kind. Methane was supplied as a fuel to the anode stream of SOFC. The internal reformer undergoes the following chemical reactions:

$$CH_4 + H_2O \leftrightarrow CO + 3H_2 (Steam\ reforming) \tag{1}$$

$$CO + H_2O \leftrightarrow CO_2 + H_2 \quad (Shifting) \tag{2}$$

Furthermore, hydrogen generated from the steam reforming and shifting reactions is used in the overall electro-chemical reactions as shown below

$$H_2 + \frac{1}{2} O_2 \leftrightarrow H_2O\ (Overall\ electro - chemical\ reaction) \tag{3}$$

The molar conversion rates of steam reforming, shifting, and overall electrochemical reactions are denoted by $a_r$, $b_r$ and $c_r$, respectively.

The molar flowrates of the flowing gases at the anode and cathode channels are calculated by the relations provided below:

$$\dot{n}_{CH_4,IN} = \dot{a}_r \tag{4}$$

$$\dot{n}_{H_2O,IN} = 2.5 \times \dot{a}_r \tag{5}$$

$$\dot{n}_{H_2,OUT} = 3\dot{a}_r + \dot{b}_r - \dot{c}_r \tag{6}$$

$$\dot{n}_{CO,OUT} = \dot{a}_r - \dot{b}_r \tag{7}$$

$$\dot{n}_{CO_2,OUT} = \dot{b}_r \tag{8}$$

$$\dot{n}_{H_2O,OUT} = \dot{n}_{H_2O,IN} - \dot{a}_r - \dot{b}_r + \dot{c}_r \tag{9}$$

$$\dot{n}_{O_2,IN} = \frac{\dot{c}_r}{2U_{O_2}} \tag{10}$$

$$\dot{n}_{O_2,OUT} = \dot{n}_{O_2,IN} - \frac{\dot{c}_r}{2} \tag{11}$$

$$\dot{n}_{N_2,OUT} = \dot{n}_{N_2,IN} \tag{12}$$

$$\dot{n}_{Ca,IN} = \dot{n}_{O_2,IN} + \dot{n}_{N_2,IN} \tag{13}$$

$$\dot{n}_{Ca,OUT} = \dot{n}_{O_2,OUT} + \dot{n}_{N_2,OUT} \tag{14}$$

$$\dot{n}_{An,IN} = \dot{n}_{CH_4,IN} + \dot{n}_{H_2O,IN} \tag{15}$$

$$\dot{n}_{An,OUT} = \dot{n}_{H_2,OUT} + \dot{n}_{CO,OUT} + \dot{n}_{CO_2,OUT} + \dot{n}_{H_2O,OUT} \tag{16}$$

The equilibrium constant of shift reaction is denoted by $K_{Shift}$ and it can be defined by

$$K_{Shift} = exp\left(-\frac{\Delta\overline{g}^0_{shift}}{\overline{R}\times T}\right) = \left[\frac{\dot{b}_r \times (3\dot{a}_r + \dot{b}_r - \dot{c}_r)}{(\dot{a}_r - \dot{b}_r)\times(\dot{n}_{H_2O,IN} - \dot{a}_r - \dot{b}_r + \dot{c}_r)}\right] \tag{17}$$

$$where, \Delta\overline{g}^0_{shift} = \Delta\overline{h}_{shift} - T \times \Delta\overline{s}_{shift} \tag{18}$$

The current density (j) is related to the hydrogen consumption molar rate ($\dot{c}_r$) by the following relation

$$j = \frac{\dot{c}_r \times 2F}{N_{cell}\times A_{cell}} \tag{19}$$

where, $A_{cell}$ and $N_{cell}$ denote area of a cell and number of cells, respectively.

The fuel utilisation factor ($UF$) can be defined as

$$UF = \frac{\dot{c}_r}{3\dot{a}_r + \dot{b}_r} \tag{20}$$

The power output produced by the SOFC stack is estimated as

$$\dot{W}_{SOFC,Stack} = N_{cell}\times V_{cell}\times j \times A_{cell} \tag{21}$$

The cell voltage ($V_{cell}$) can be estimated as

$$V_{cell} = V_N - (V_{act} + V_{conc} + V_{ohm}) \tag{22}$$

where, $V_N$, $V_{act}$, $V_{conc}$ ,and $V_{ohm}$ are Nernst voltage, activation loss, concentration loss, and ohmic loss, respectively. The Nernst voltage can be estimated as follows

$$V_N = -\frac{\Delta\overline{g}^0}{2F} + \frac{\overline{R}T_{SOFC}}{2F} ln\left(\frac{a_{H_2,OUT}\times\sqrt{a_{O_2,OUT}}}{a_{H_2O,OUT}}\right) \tag{23}$$

where,

$$a_{H_2,OUT} = \frac{P_{H_2,OUT}}{P_0}\ ;\ a_{H_2O,OUT} = \frac{P_{H_2O,OUT}}{P_0};\ a_{O_2,OUT} = \frac{P_{O_2,OUT}}{P_0} \tag{24}$$

Equations used for calculation of different voltage losses are provided in Table 1.

### 2.3. Supercritical carbon dioxide cycle

The waste heat from the gas heater drives a recuperated supercritical $CO_2$ power cycle with single-stage compression. It has been demonstrated that recuperated s-$CO_2$ cycle outperforms that of a simple s-$CO_2$ cycle in terms of thermodynamic performance [34]. In this investigation, a recuperated supercritical $CO_2$ power cycle is chosen. The power generated by turbine (SCT) is obtained by the following equation

$$\dot{W}_{SCT} = \dot{m}_{CO_2}(h_{in} - h_{out}) \tag{25}$$

where, $\dot{m}_{CO_2}$ and h represent mass flowrate of carbon dioxide and enthalpy respectively. The subscripts "in" and "out" represents inlet and outlet streams

The estimation of the auxiliary power requirement in the $CO_2$ compressor (SCC) is done using the following equation.

$$\dot{W}_{SCC} = \dot{m}_{CO_2}(h_{out} - h_{in}) \tag{26}$$

### 2.4. Economic analysis

Table 2 shows the capital costs of various equipment as well as other important data for economic analysis.

The total capital cost (CAPEX) is calculated by adding all of the investment costs of the various components, and it is expressed by the equation below.

$$CAPEX = \sum_i Z_{CAP_i} \tag{27}$$

where, $Z_{CAP_i}$ is the investment cost of ith component.

The discount rate is set at 3%, and the lifespan is chosen at 30 years. Annual operation and maintenance costs are estimated to be 2.5% of CAPEX. SOFC and other components must be replaced on a regular basis in the system. The annual replacement budget is estimated to equal 5% of CAPEX. Over a 30-year timeline, a total of 3 SOFC stacks will be required, assuming a lifespan of 10 years for each stack. As illustrated in the following equation, the total yearly cost of the system is the summation of the yearly capital cost, annual operational and maintenance cost, annual replacement cost, and annual fuel cost.

**Table 2**
Cost of different components.

| Description | Value | Unit | Ref. |
|---|---|---|---|
| Solid oxide fuel cell | 4500 | €/kW | [35] |
| Pump + Compressor + Heat Exchanger + Pipe works | 202.5 | \$/kW | [36] |
| s-$CO_2$ cycle | 2000 | \$/kW | [37] |
| Methane cost | 7.21 | p/kWh | [38] |

**Table 1**
Different voltage losses.

| Type | Equations | Ref |
|---|---|---|
| Activation loss | $V_{act} = V_{act,Anode} + V_{act,Cathode}$ | [31,32] |
| | $V_{act,Anode} = \frac{\overline{R}\times T}{F}\left(sin\ h^{-1}\frac{j}{2j_{OA}}\right)$ | |
| | $V_{act,Cathode} = \frac{\overline{R}\times T}{F}\left(sin\ h^{-1}\frac{j}{2j_{OC}}\right)$ | |
| Concentration loss | $V_{conc} = V_{conc,Anode} + V_{conc,Cathode}$ | [33] |
| | $V_{conc,Anode} = \frac{\overline{R}T_{SOFC}}{2F}\left(ln\left(1+\frac{P_{H_2,OUT}\times j}{P_{H_2O,OUT}\times j_{AS}}\right) - ln\left(1-\frac{j}{j_{AS}}\right)\right)$ | |
| | $V_{conc,Cathode} = -\left(\frac{\overline{R}T}{4F}ln\left(1-\frac{j}{j_{CS}}\right)\right)$ $j_{AS} = \frac{2F\times P_{H_2,OUT}\times D_{Anode,eff}}{\overline{R}\times T\times L_{Anode}}$ | |
| | $j_{CS} = \frac{4F\times P_{O_2,OUT}\times D_{Cathode,eff}}{\left(\left(\frac{P_4 - P_{O_2,4}}{P_4}\right)\times\overline{R}\times T\times L_{Cathode}\right)}$ | |
| Ohmic loss | $V_{ohm} = (R_C + \sum_k \rho_k L_k)\times j$ | [31] |
| | $\rho_{Anode} = (95\times10^6/T * exp(-1150/T))^{-1}$ | |
| | $\rho_{Cathode} = (42\times10^6/T * exp(-1200/T))^{-1}$ | |
| | $\rho_{Electrolyte} = (3.34\times10^4/T * exp(-10300/T))^{-1}$ | |
| | $\rho_{Interconnect} = \left(9.3\times\frac{10^6}{T} * exp(-1100/T)\right)^{-1}$ | |

$$COST_{Annual} = CAPEX_{Annual} + OPEX_{Annual} + REP_{Annual} + FUEL_{Annual} \tag{28}$$

### 2.5. Performance indices

The net power generated by the investigated SOFC-s$CO_2$ system is determined by the following relation

$$\dot{W}_{net} = \dot{W}_{SOFC,Stack} + \dot{W}_{SCT} - \dot{W}_{Auxiliary} \tag{29}$$

The power consumed by the auxiliary components ($\dot{W}_{Auxiliary}$) of the model is calculated using the following equation

$$\dot{W}_{Auxiliary} = \dot{W}_{FC} + \dot{W}_{BA} + \dot{W}_{SCC} + \dot{W}_{Pump} \tag{30}$$

where, $\dot{W}_{FC}$, $\dot{W}_{BA}$, $\dot{W}_{SCC}$, and $\dot{W}_{Pump}$ are the power consumed by the fuel compressor, air blower, $CO_2$ compressor and pump respectively.

The net efficiency of the proposed system ($\eta_{sys}$) is estimated by the following equation

$$\eta_{sys} = \frac{\dot{W}_{net}}{\dot{m}_{fuel} \times LHV_{fuel}} \tag{31}$$

The levelised cost of energy (LCOE) for the system is estimated using the following equation

$$LCOE = \frac{COST_{Annual}\ (£)}{Total\ Energy\ Production\ (kWh)} \tag{32}$$

## 3. Response surface methodology

Response surface methodology was utilised in this work to construct a functional relationship between objective responses and specified input variables. Furthermore, interactive effects of selected input variables on the objective responses were analysed. The Box-Behnken design of experiment method, proposed by George E. P. Box and Donald Behnken, is utilised to design the numerical design [39]. The selected input variables were current density (j), fuel utilisation factor (UF) and operating temperature of the fuel cell ($T$), respectively. The efficiency of the system and the levelised cost of electricity (LCOE) were selected as the objective responses. A full quadratic model as shown in equation (33) can be applied to correlate the objective responses and the input variables.

$$Y_i = a_0 + \sum_{i=1}^{k} a_i X_i + \sum_{i=1}^{k} a_{ii} X_i^2 + \sum_{i=1}^{k-1} \sum_{j=i+1}^{k} a_{ij} X_i X_j + e \tag{33}$$

where, "$Y_i$" is response, "X" is factor, "k" is the number of factors, $a_0$, $a_i$, $a_{ii}$, $a_{ij}$ are unknown regression coefficients, respectively.

Each input variable was specified into three levels, coded +1, 0, and −1, respectively, according to the minimum level, medium level, and maximum level as shown in Table 3. 15 runs were selected as per the Box-Behnken design, using Minitab 21.1 software. The simulation is performed according to the Box-Behnken design and responses are estimated and presented in Table 3.

## 4. Results and discussion

In this section, the SOFC model is first validated. Furthermore, sensitivity analysis of the proposed system has been performed, and the response surface methodology is being utilised to further investigate and optimise the performance of the system. The technical input parameters required for the analysis are provided in Table 4. The flowchart of the analysis adopted in this study is shown in Fig. 2.

**Table 3**
Investigated input variables used in the DOE and their levels.

| Independent variables | Levels | | |
|---|---|---|---|
| | −1 | 0 | +1 |
| Current density (A/m$^2$) | 1500 | 2500 | 3500 |
| Fuel utilisation factor | 0.7 | 0.8 | 0.9 |
| Operating temperature fuel cell (°C) | 750 | 850 | 900 |

### 4.1. Model validation

Solid oxide fuel cell components play a crucial role in the proposed system, and it is essential to validate their performance using experimental data. In this study, the results obtained from the current SOFC model are compared with the experimental findings reported by Singhal et al. [40]. The experiment utilised zirconia doped with about 10 mol.% yttria as the electrolyte. For validation purposes, the fuel mixture used consisted of 89% hydrogen and 11% water, while the cell temperature was maintained at 1000 °C. The model was appropriately adjusted to achieve a fuel utilisation of 85% during the validation process. Fig. 3 demonstrates that the results obtained from the current SOFC model exhibit excellent agreement with the experimental data, with a maximum discrepancy of 3.7%.

### 4.2. Sensitivity analysis

The variations in efficiency of the integrated energy system with current density are shown in Fig. 4a. The system's net power production rises with increased current densities. The energy efficiency declines with increasing current density because the rate of growth in net power output is less than the rate of increase in input energy. With reference to Fig. 4b, a higher level of system efficiency is achieved when the fuel utilisation factor rises from 0.7 to 0.9. Additionally, it can be shown in Fig. 4c that the system's efficiency falls when the fuel cell's working temperature rises.

Fig. 5a depicts the LCOE fluctuations of the system with current density. It has been observed that when current density increase, the LCOE reduces. As illustrated in Fig. 5a, this is related to a drop in system efficiency. According to Fig. 5b, increasing the fuel utilisation factor from 0.7 to 0.9 lowers the LCOE. It is because system efficiency increases with increasing UF levels. In addition, as shown in Fig. 5c, when the operating temperature of the fuel cell increases, so does the LCOE of the system, as system efficiency drops at higher cell temperatures.

**Table 4**
Input parameters for technical analysis [31].

| Components | Parameters | Values | Units |
|---|---|---|---|
| SOFC | Area of a cell | 0.01 | m$^2$ |
| | Exchange current density of cathode | 2500 | A/m$^2$ |
| | Exchange current density of anode | 6500 | A/m$^2$ |
| | Thickness of electrolyte | 0.00001 | m |
| | Thickness of anode | 0.0005 | m |
| | Thickness of cathode | 0.00005 | m |
| | Thickness of interconnect | 0.003 | m |
| | Effective gas diffusivity through anode | 0.000005 | m$^2$/s |
| | Effective gas diffusivity through cathode | 0.00002 | m$^2$/s |
| | Steam to carbon ratio | 2.5 | – |
| | Pressure drop in SOFC | 2 | % |
| | Pressure drop at afterburner | 3 | % |
| Fuel compressor | Isentropic efficiency | 85 | % |
| Air blower | Isentropic efficiency | 85 | % |
| Pump | Isentropic efficiency | 85 | % |
| s-$CO_2$ cycle | Maximum pressure of the cycle | 12000 | kPa |
| | Minimum pressure of the cycle | 7500 | kPa |
| | Turbine inlet temperature | 150 | °C |
| | Pinch point temperature difference at the regenerator | 5 | °C |

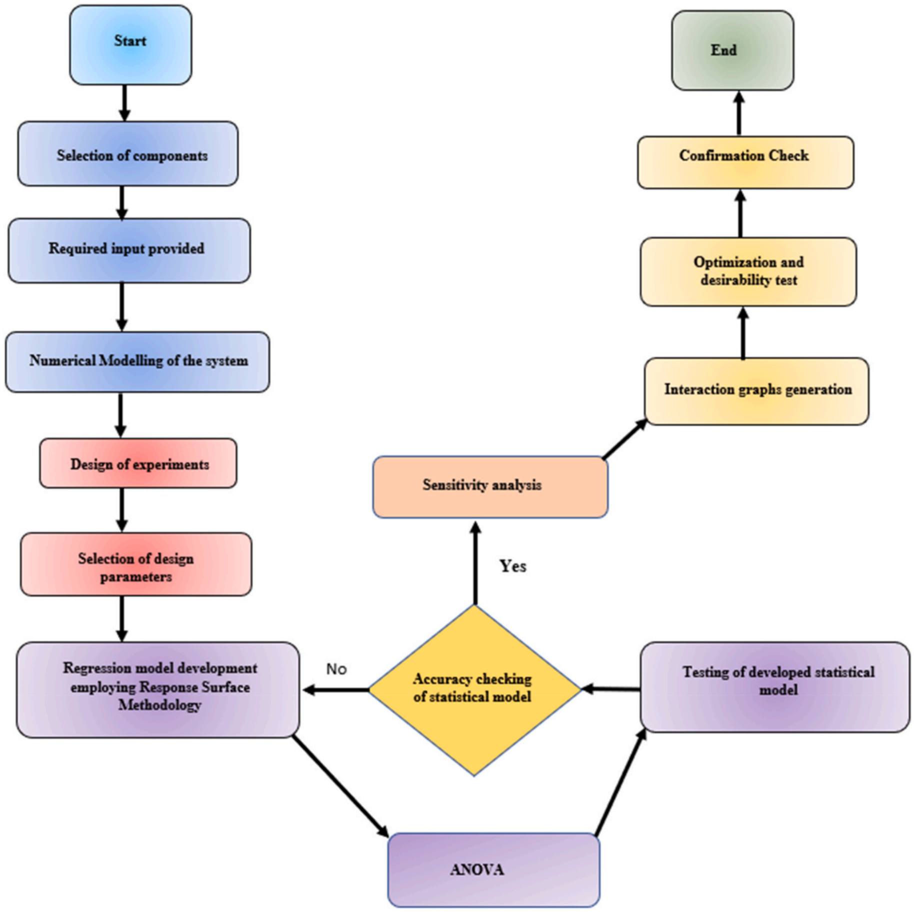


**Fig. 2.** Flowchart of the analysis.

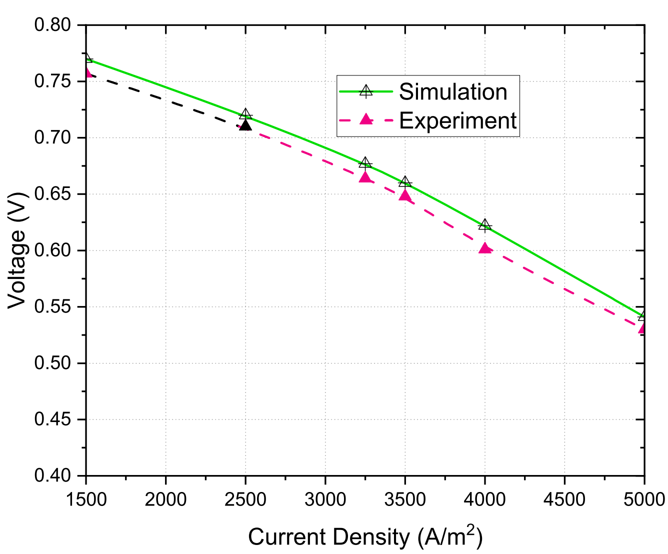


**Fig. 3.** Solid oxide fuel cell model validation.

### 4.3. Analysis of variance (ANOVA)

Table 5 shows the results from ANOVA for energy efficiency of the system as the one objective response. The p-value is an important model parameter. A p-value greater than 0.05 is deemed insignificant. Table 5 shows that the model's p-value is 0 with a larger F-value (21744.01), indicating that the model is significant. Table 5 further reveals that each term of the regression model is significant, i.e., linear, square, and 2-way interaction for system efficiency. Fig. 6 depicts the Pareto chart for standardised effects for the response efficiency of the system. Given that every bar crosses the reference line 2.4, implying that all of the terms are meaningful.

Table 6 shows the results from ANOVA for LCOE of the system as the one objective response. The fact that the model's p-value is 0 and its F-value is larger (1488.51) indicates that the model is significant. Table 6 further demonstrates the significance of each parameter in the regression model, including the linear, square, and two-way interactions for LCOE. The Pareto chart for standardised effects for the response LCOE of the system is depicted in Fig. 7. All the bars are seen to cross the reference line at 2.4, which implies that all the terms are significant.

The regression models for the two objective responses, namely system efficiency and LCOE, were generated based on the ANOVA results. The regression equations for the system's energy efficiency and LCOE determined from ANOVA analysis are shown below.

$$\eta_{sys}(\%) = -118.07 + 0.004930 \times j + 356.23 \times UF + 0.07053 \times T - 145.10 \times UF^2 - 0.000024 \times T^2 - 0.009500 \times j \times UF - 0.08175 \times UF \times T \tag{34}$$

$$LCOE\left(\frac{£}{kWh}\right) = 0.6782 - 0.000020 \times j - 0.9301 \times UF - 0.000240 \times T + 0.4348 \times UF^2 + 0.000023 \times j \times T + 0.000139 \times UF \times T \tag{35}$$

For the system efficiency model, higher values of $R^2_{adj}$ and $R^2_{pred}$ are observed, viz. 99.99% and 99.98%, respectively. Similarly, the $R^2_{adj}$ and

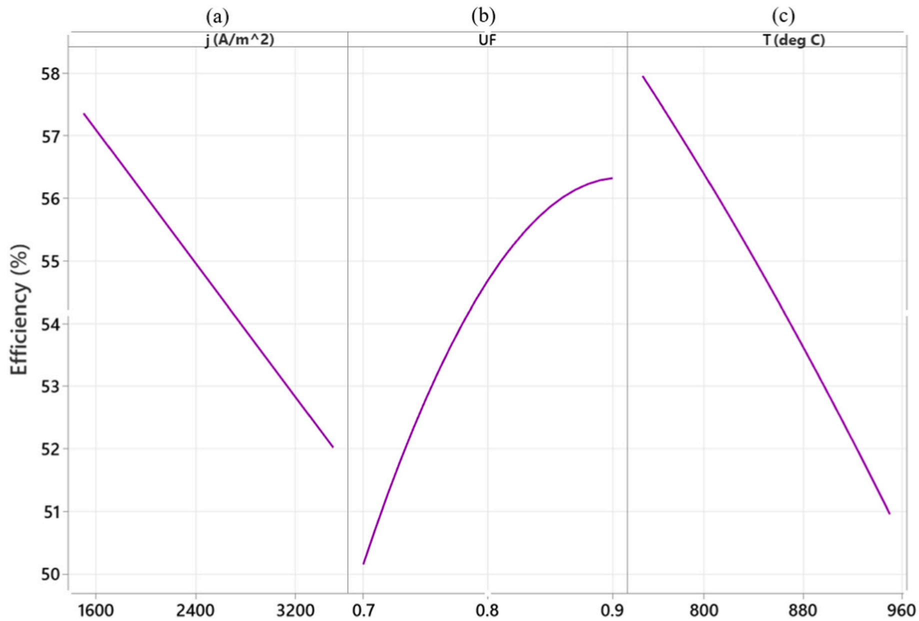


**Fig. 4.** Influence of input parameters on efficiency of the system ($\eta_{sys}$), a) Current density (j), b) Fuel utilisation factor (UF), c) operating temperature of fuel cell (T).

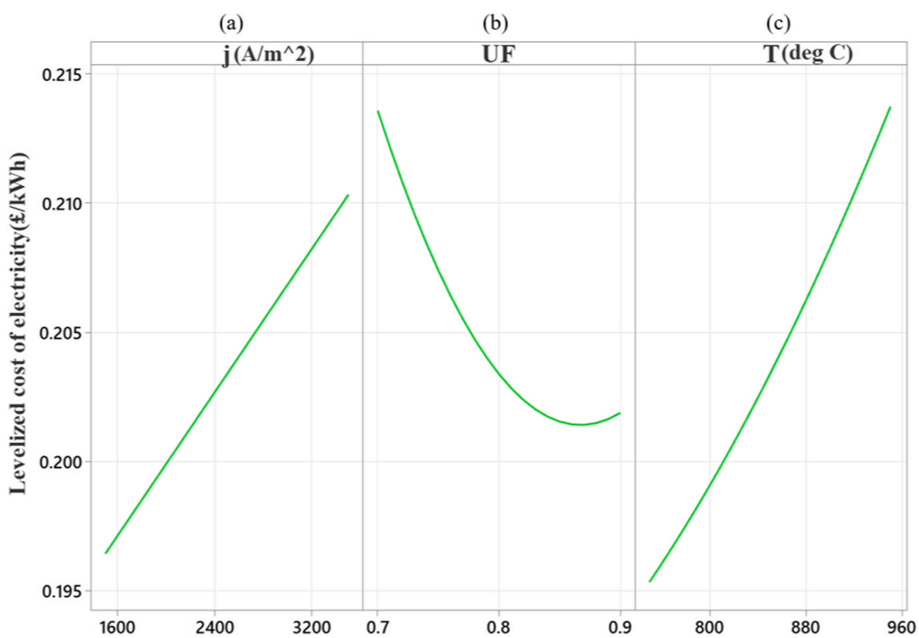


**Fig. 5.** Influence of input parameters on LCOE of the system; a) Current density (j), b) Fuel utilisation factor (UF), c) operating temperature of fuel cell (T).

$R^2_{pred}$ values for the LCOE model are higher, 99.88% and 99.53%, respectively. It suggests that models exhibit a greater degree of accuracy.

### 4.4. Response surface methodology and numerical model comparison

Table 7 displays the system efficiency and LCOE values for various current densities, fuel utilisation factors, and fuel cell operating temperatures. It also shows the comparative results obtained between the RSM and the numerical model. For both system efficiency and LCOE, the root mean square error is estimated to be 0.0274 and 0.0002, respectively.

### 4.5. Interaction effect of decision parameters on objective responses

The interaction effect of UF and 'j' on the efficiency of the system has been shown in Fig. 8. The maximum value of efficiency (greater than 58%) has been observed at a high value of UF (more than 0.82) and low 'j' (less than 2000 A/m$^2$) and minimum efficiency (less than 41%) is observed when UF is less than 0.74 and 'j' is more than 2600 A/m$^2$. The interaction effect of 'T' and 'j' on the efficiency of the system has been shown in Fig. 9. The maximum value of efficiency (greater than 60%) has been observed at lower values of T (less than 770 °C) and low 'j' (less than 1650 A/m$^2$) and minimum efficiency (less than 50%) is observed when T is higher than 900 °C and 'j' is more than 2850 A/m$^2$. The interaction effect of 'T' and 'UF' on the efficiency of the system has been shown in Fig. 10. The maximum value of efficiency (greater than 60%) has been observed at a lower value of T (less than 760 °C) and a high 'UF'

**Table 5**
ANOVA for energy efficiency of the system.

| Source | DF | Seq SS | Contribution | Adj SS | Adj MS | F-Value | P-Value |
|---|---|---|---|---|---|---|---|
| Model | 7 | 245.206 | 100.00% | 245.206 | 35.0294 | 21744.01 | 0.000 |
| Linear | 3 | 231.037 | 94.22% | 231.037 | 77.0124 | 47804.45 | 0.000 |
| j | 1 | 57.031 | 23.26% | 57.031 | 57.0312 | 35401.36 | 0.000 |
| UF | 1 | 76.076 | 31.02% | 76.076 | 76.0761 | 47223.23 | 0.000 |
| T | 1 | 97.930 | 39.94% | 97.930 | 97.9300 | 60788.75 | 0.000 |
| Square | 2 | 7.885 | 3.22% | 7.885 | 3.9425 | 2447.26 | 0.000 |
| UF*UF | 1 | 7.678 | 3.13% | 7.820 | 7.8196 | 4853.94 | 0.000 |
| T*T | 1 | 0.207 | 0.08% | 0.207 | 0.2068 | 128.37 | 0.000 |
| 2-Way Interaction | 2 | 6.283 | 2.56% | 6.283 | 3.1416 | 1950.11 | 0.000 |
| j*UF | 1 | 3.610 | 1.47% | 3.610 | 3.6100 | 2240.86 | 0.000 |
| UF*T | 1 | 2.673 | 1.09% | 2.673 | 2.6732 | 1659.37 | 0.000 |
| Error | 7 | 0.011 | 0.00% | 0.011 | 0.0016 | | |
| Lack-of-Fit | 5 | 0.011 | 0.00% | 0.011 | 0.0023 | * | * |
| Pure Error | 2 | 0.000 | 0.00% | 0.000 | 0.0000 | | |
| Total | 14 | 245.217 | 100.00% | | | | |

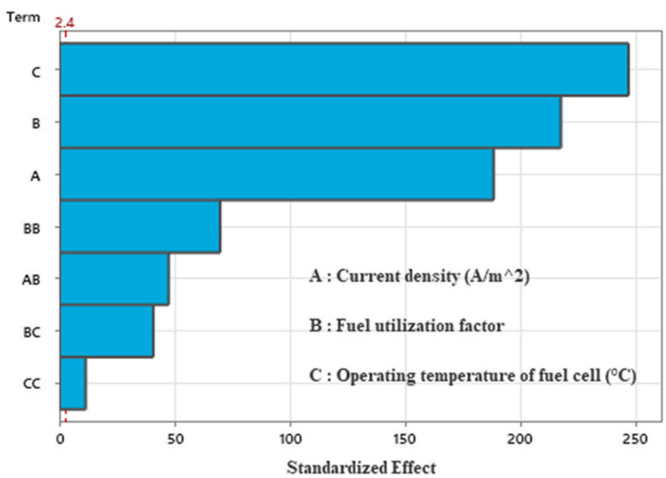


**Fig. 6.** Pareto chart for standardised effects for response efficiency of the system.

(greater than 0.87) and a minimum efficiency (less than 48%) is observed when T is higher than 925 °C and 'UF' is less than 0.72.

The interaction effect of 'T' and 'j' on the LCOE of the system has been shown in Fig. 11. The minimum value of LCOE (less than 0.190 £/kWh) has been observed at lower values of j (less than 1550 A/m$^2$) and low 'T' (less than 750 °C) and maximum LCOE (higher than 0.22 £/kWh) is observed when T is higher than 935 °C and 'j' is higher than 3250 A/m$^2$. The interaction effect of 'UF' and 'j' on the LCOE of the system has been shown in Fig. 12. The minimum value of LCOE (lesser than 0.195 £/kWh)) has been observed at lower values of current density (less than 1750 A/mˆ2) and high 'UF' (greater than 0.82) and higher LCOE (more than 0.215£/kWh) is observed when j is higher than 3400 A/mˆ2 and 'UF' is less than 0.72. The interaction effect of 'j' and 'UF' on the LCOE of the system has shown in Fig. 13. The lowest LCOE (less than 0.195£/kWh) has been seen when T is less than 775 °C and the 'UF' is more than 0.81, while the highest LCOE (more than 0.22£/kWh) has been observed when T is larger than 925 °C and the 'UF' is less than 0.72.

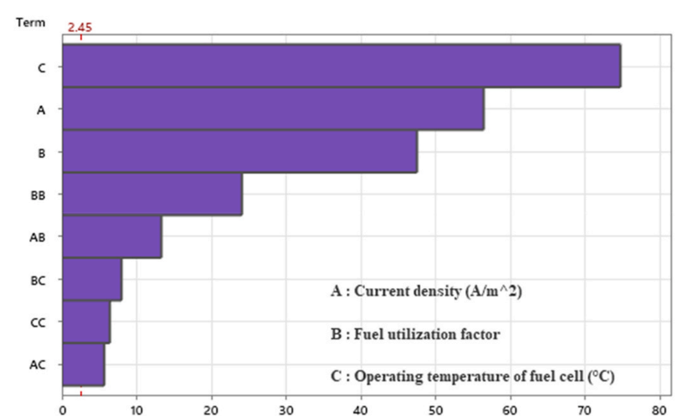


**Fig. 7.** Pareto chart for standardised effects for LCOE of the system.

**Table 6**
ANOVA for LCOE of the system.

| Source | DF | Seq SS | Contribution | Adj SS | Adj MS | F-Value | P-Value |
|---|---|---|---|---|---|---|---|
| Model | 8 | 0.001442 | 99.95% | 0.001442 | 0.000180 | 1488.51 | 0.000 |
| Linear | 3 | 0.001336 | 92.60% | 0.001336 | 0.000445 | 3677.65 | 0.000 |
| J | 1 | 0.000386 | 26.76% | 0.000386 | 0.000386 | 3188.42 | 0.000 |
| UF | 1 | 0.000273 | 18.95% | 0.000273 | 0.000273 | 2257.46 | 0.000 |
| T | 1 | 0.000676 | 46.89% | 0.000676 | 0.000676 | 5587.06 | 0.000 |
| Square | 2 | 0.000073 | 5.05% | 0.000073 | 0.000036 | 301.02 | 0.000 |
| UF*UF | 1 | 0.000068 | 4.71% | 0.000070 | 0.000070 | 579.97 | 0.000 |
| T*T | 1 | 0.000005 | 0.34% | 0.000005 | 0.000005 | 41.02 | 0.001 |
| 2-Way Interaction | 3 | 0.000033 | 2.29% | 0.000033 | 0.000011 | 91.03 | 0.000 |
| j*UF | 1 | 0.000021 | 1.49% | 0.000021 | 0.000021 | 177.12 | 0.000 |
| j*T | 1 | 0.000004 | 0.27% | 0.000004 | 0.000004 | 32.16 | 0.001 |
| UF*T | 1 | 0.000008 | 0.54% | 0.000008 | 0.000008 | 63.81 | 0.000 |
| Error | 6 | 0.000001 | 0.05% | 0.000001 | 0.000000 | | |
| Lack-of-Fit | 4 | 0.000001 | 0.05% | 0.000001 | 0.000000 | * | * |
| Pure Error | 2 | 0.000000 | 0.00% | 0.000000 | 0.000000 | | |
| Total | 14 | 0.001442 | 100.00% | | | | |

**Table 7**
Design matrix with numerical model results and response surface methodology projected values.

| Std Order | Run Order | Pt Type | Blocks | Input variables | | | $\eta_{sys}$ (%) | | LCOE (£/kWh) | |
|---|---|---|---|---|---|---|---|---|---|---|
| | | | | Current density (A/m$^2$) | Fuel utilisation factor | Fuel cell Operating Temperature (°C) | RSM | Numerical Model | RSM | Numerical Model |
| 14 | 1 | 0 | 1 | 2500 | 0.8 | 850 | 54.687 | 54.69 | 0.20338 | 0.20320 |
| 2 | 2 | 2 | 1 | 3500 | 0.7 | 850 | 48.433 | 48.40 | 0.21820 | 0.21825 |
| 10 | 3 | 2 | 1 | 2500 | 0.9 | 750 | 60.401 | 60.40 | 0.19246 | 0.19217 |
| 9 | 4 | 2 | 1 | 2500 | 0.7 | 750 | 52.598 | 52.62 | 0.20693 | 0.20658 |
| 8 | 5 | 2 | 1 | 3500 | 0.8 | 950 | 48.283 | 48.27 | 0.22167 | 0.22176 |
| 5 | 6 | 2 | 1 | 1500 | 0.8 | 750 | 60.621 | 60.55 | 0.18939 | 0.18957 |
| 4 | 7 | 2 | 1 | 3500 | 0.9 | 850 | 52.701 | 52.69 | 0.21115 | 0.21113 |
| 12 | 8 | 2 | 1 | 2500 | 0.9 | 950 | 51.768 | 51.75 | 0.21363 | 0.21369 |
| 3 | 9 | 2 | 1 | 1500 | 0.9 | 850 | 59.941 | 59.97 | 0.19262 | 0.19286 |
| 11 | 10 | 2 | 1 | 2500 | 0.7 | 950 | 47.236 | 47.24 | 0.22254 | 0.22254 |
| 15 | 11 | 0 | 1 | 2500 | 0.8 | 850 | 54.688 | 54.69 | 0.20338 | 0.20320 |
| 7 | 12 | 2 | 1 | 1500 | 0.8 | 950 | 53.623 | 53.65 | 0.20580 | 0.20563 |
| 1 | 13 | 2 | 1 | 1500 | 0.7 | 850 | 51.873 | 51.88 | 0.20894 | 0.20924 |
| 13 | 14 | 0 | 1 | 2500 | 0.8 | 850 | 54.688 | 54.69 | 0.20338 | 0.20320 |
| 6 | 15 | 2 | 1 | 3500 | 0.8 | 750 | 55.281 | 55.33 | 0.20130 | 0.20175 |

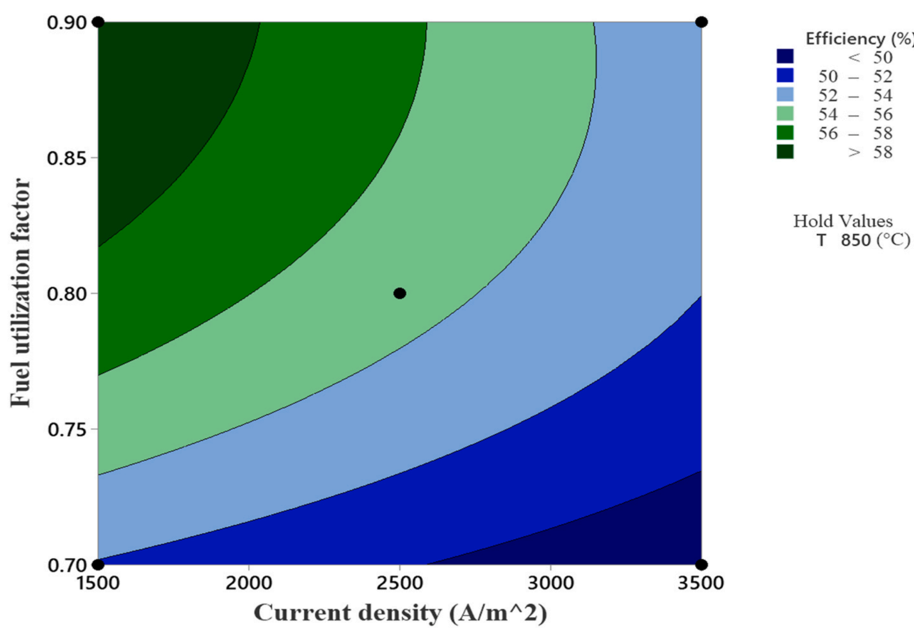


**Fig. 8.** Interaction consequence of UF and j on efficiency of the system.

## 4.6. Multi-objective optimisation

In this section, multi-objective optimisation was carried out utilising the Minitab software's response optimiser tool. Table 8 shows the optimisation constraints as well as the objectives.

In Minitab software, every response is transformed to a dimensionless desirability value (d). The value of 'd' ranges between 0 and 1. The values of 1 and 0 indicate desirable results and unacceptable results, respectively. The combined desirability (D) can be defined as follows [41].

$$D = [d_1(y_1) \times d_2(y_2) \times d_3(y_3) \times \ldots\ldots\ldots\ldots\ldots d_n(y_n)]^{1/n} \tag{36}$$

where, n is the number of responses.

Individual desirability of all the responses is found to be 1. Thus, combined desirability is found to be 1. Thus, the model generates acceptable results. The optimum conditions are shown in Fig. 14 to be j = 1500 A/m$^2$, UF = 0.9 and T = 750 °C. In addition, the RSM optimiser predicted outcomes are validated using the numerical model and are shown in Table 9. The model estimated optimum efficiency and LCOE of 63.97% and 0.1848 £/kWh. The model predicted an optimum efficiency and LCOE of 63.97% and 0.1848 £/kWh, respectively. The RSM optimiser estimated the best efficiency and LCOE of 64.02% and 0.1842 £/kWh, respectively. The LCOE and efficiency percentages of error are calculated to be 0.32% and 0.08%, respectively.

## 4.7. Performance comparison

Table 10 compares the performance of the proposed system with conventional natural gas fired combined cycle (NGCC) and combined cycle gas turbine (CCGT) power plants. NGCC plants are the most conventional electric power generation pathway all around the world using natural gas as the energy input. Centralised power stations powered by NGCC are typically several megawatts in size. The suggested small-scale decentralised district power generation system has the highest efficiency of 64%. Compared to other conventional NGCC system, the proposed system offers competitive energetic efficiency. Furthermore, NGCC systems are not suitable for modest scale commercial operation. The use

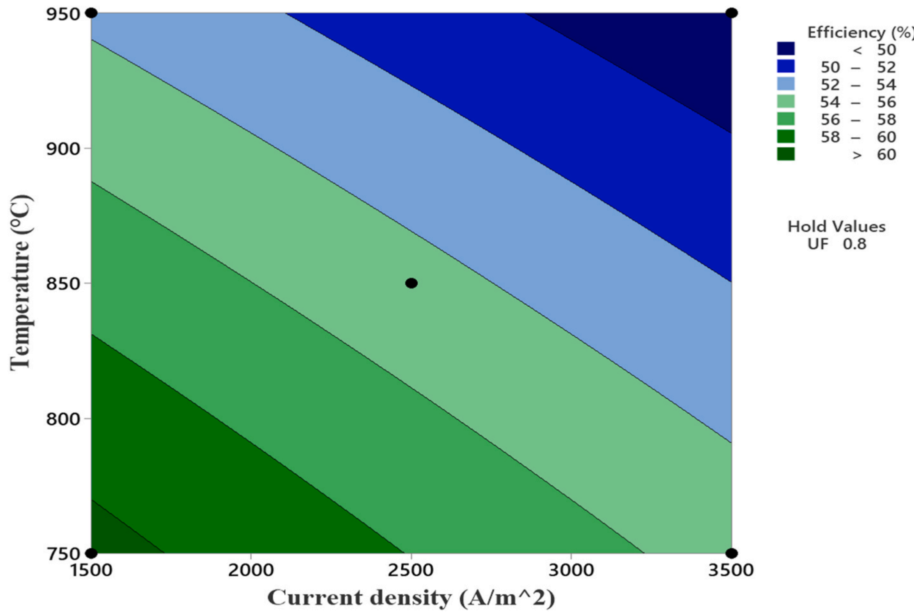


**Fig. 9.** Interaction consequence of T and j on efficiency of the system.

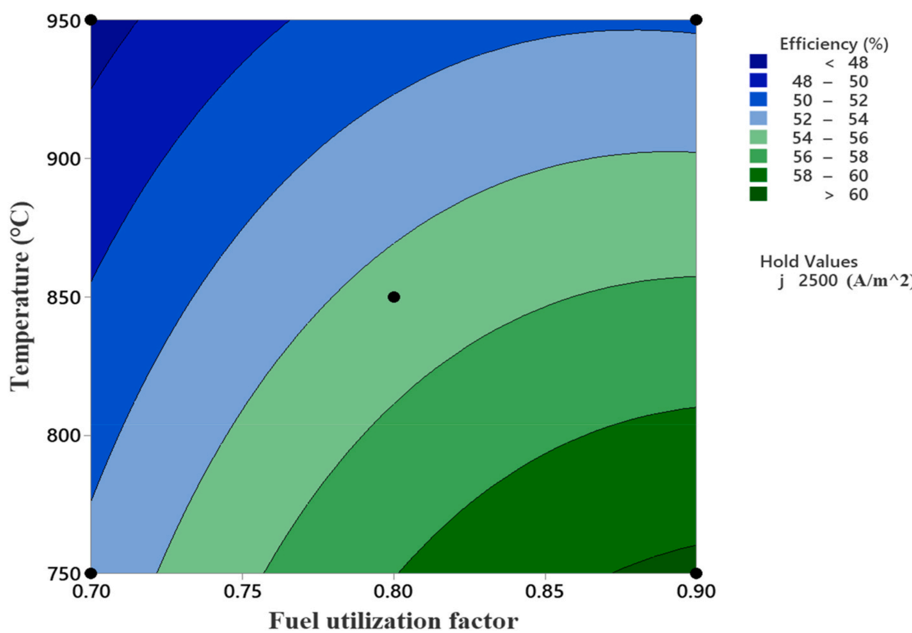


**Fig. 10.** Interaction consequence of T and UF on efficiency of the system.

of directly fired gas turbines and the contact of the gas turbine blades with combustion gases are characteristics of the classic CCGT and NGCC systems. These issues are not present in the fuel-cell-based technology employed in this investigation. Additionally, because fuel cells produce less noise while operating, the fuel cell integrated system is preferable. The proposed integrated energy system is superior to other traditional natural gas fuelled gas turbine systems. However, with the development of the material research and development once the specific cost of the SOFC would achieve its lowest price (DOE target 900$/kW [42]) the overall levelised cost of electricity of the proposed power generation system would become very much competitive compared to the conventional NGCC systems. Moreover, the proposed system offers better performance in terms of $CO_2$ emissions with 311.45 kg/MWh, which is lower than CCGT [43–45] and NGCC [46] plants.

### 4.8. Modification of the system using green hydrogen as a fuel

Typically, green hydrogen is generated by utilising renewable energy to operate an electrolysis process that separates hydrogen and oxygen from water [47]. The proposed system has been modified, and green hydrogen has been supplied at the optimum design configuration. The modified configuration is shown in Fig. 15. The system efficiency has been improved substantially, and it is estimated to be 73.37%. An approximate 10% efficiency improvement has been found compared to the methane-fuelled option. However, the levelised cost of electricity will be highly dependent on the green hydrogen price. Presently, there is no consensus on the price of green hydrogen, and green hydrogen is available at variable ranges in different geographical locations. The cheapest green hydrogen, for example, is currently available in some Middle Eastern countries, including Qatar (3.51 $/kg), Saudi Arabia

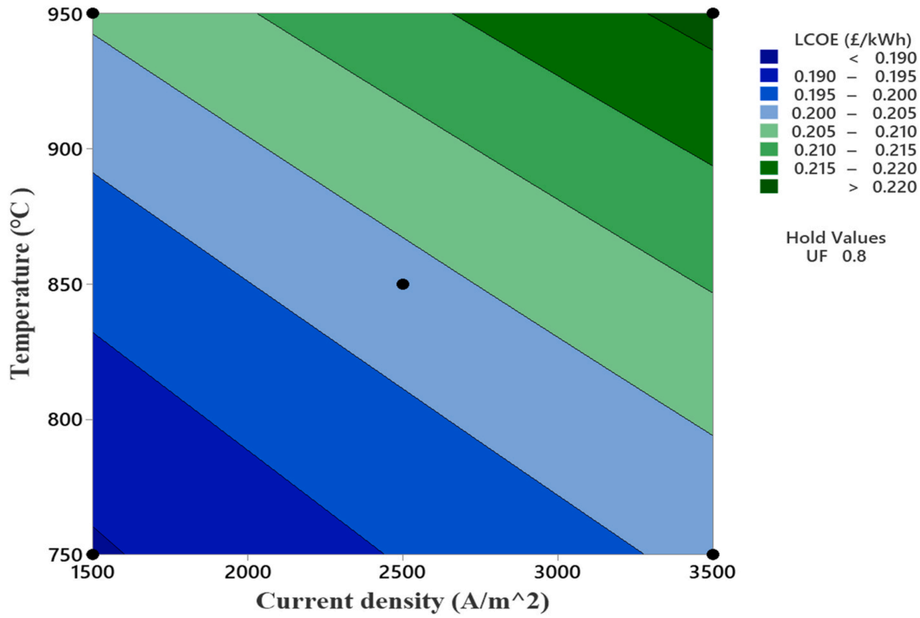


**Fig. 11.** Interaction consequence of T and j on efficiency of the system.

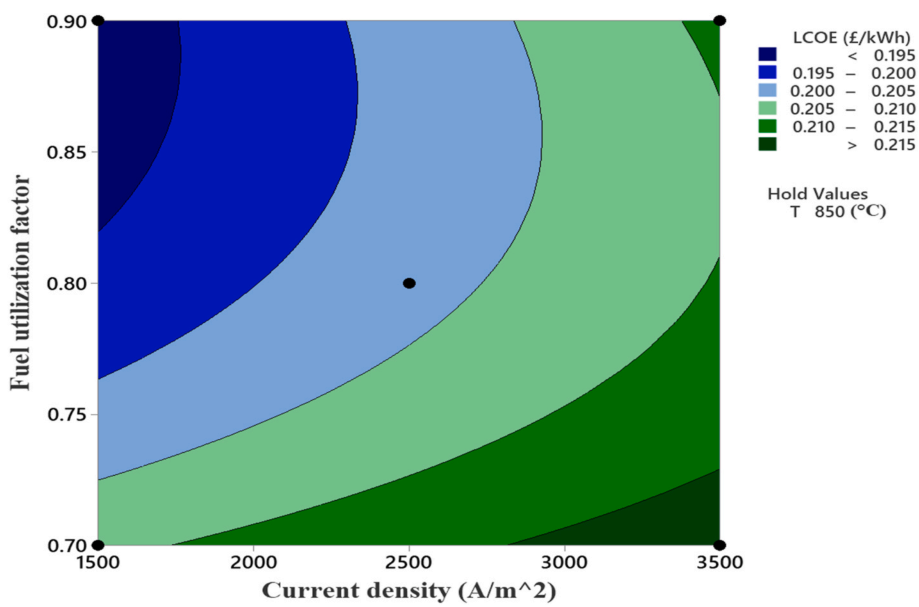


**Fig. 12.** Interaction consequence of UF and j on LCOE of the system.

(4.23 $/kg), and the UAE (6.45 $/kg) using PEM electrolysers [48]. Green hydrogen is substantially more expensive in the United Kingdom, costing 17.57 $/kg using an alkaline electrolyser and 20.81 $/kg using a PEM electrolyser, respectively [48]. Thus, it is important to conduct a sensitivity analysis for estimating LCOE with the variation of cost of green hydrogen.

Fig. 16 depicts the variation of cost of green hydrogen on the LCOE. The minimum LCOE of the system is estimated to be 0.2123 £/kg, which is approximately 15% higher than the methane-based option. It is important to emphasise that the modified system emits no $CO_2$ into the atmosphere because it is driven by hydrogen.

## 5. Conclusions

This study proposes and investigates a hybrid power generating system that integrates a SOFC and a recuperated s-$CO_2$ cycle at the downstream for waste heat recovery. The proposed system has been analysed from both thermodynamic and economic perspectives, and the results have been thoroughly discussed. Multi-objective optimisation of the system has also been performed using Response Surface Methodology (RSM). The proposed system's comparative optimum performance has been investigated taking into account the effects of the current density, fuel utilisation factor, fuel cell operating temperature. Furthermore, the proposed SOFC-s-$CO_2$ configuration was fuelled by green hydrogen, and the system's performance was investigated. Some of the key findings are as follows:

- The estimated maximum energy efficiency of the system is around 64%, at $j = 1500$ A/m$^2$, $T_{cell} = 750$ K, UF = 0.9.
- The minimum levelised cost of electricity of the proposed power plant is computed as 0.18 £/kWh under the same optimal operating conditions.

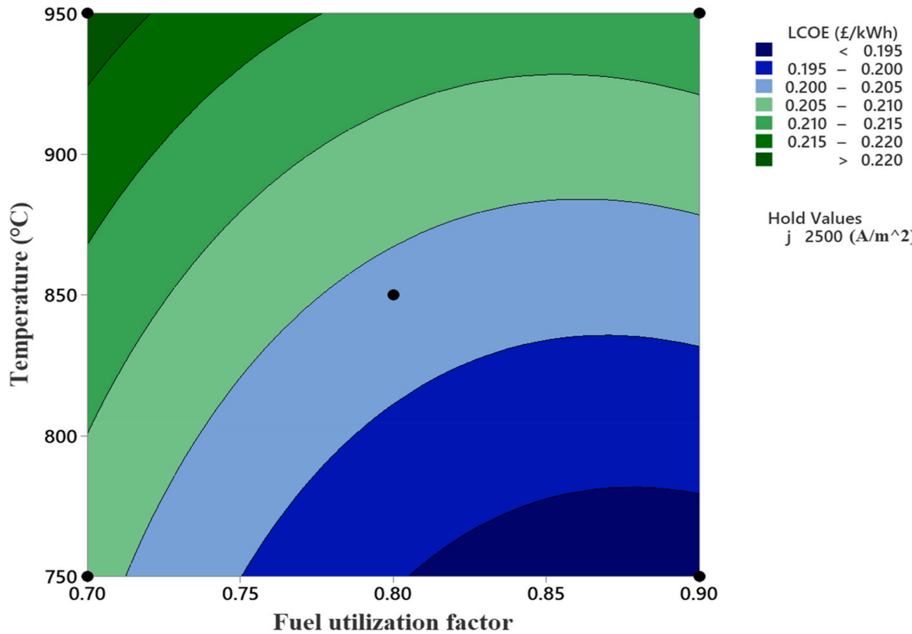


**Fig. 13.** Interaction consequence of T and UF on LCOE of the system.

**Table 8**
Optimisation constraints and objectives.

| Parameters | Range/objective |
|---|---|
| Current density (A/m$^2$) | 1500–3500 |
| Fuel utilisation factor | 0.70–0.90 |
| Operating temperature of fuel cell (°C) | 750–950 |
| Energy efficiency (%) | Maximise |
| Levelised cost of energy (£/kWh) | Minimise |

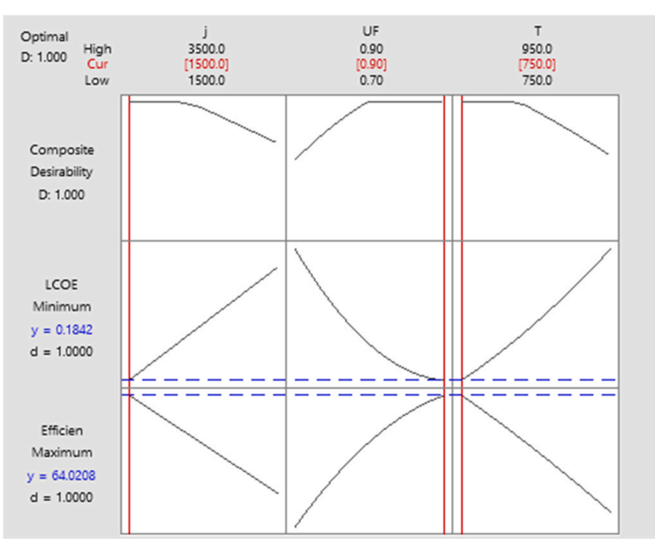


**Fig. 14.** Response optimiser plot generated using Minitab.

**Table 9**
Validation table.

| Efficiency (%) | | Error (%) | LCOE (£/kWh) | | Error (%) |
|---|---|---|---|---|---|
| Model | RSM | | Model | RSM | |
| 63.97 | 64.0208 | 0.08 | 0.1848 | 0.1842 | 0.32 |

**Table 10**
Performance comparisons between the proposed plant and conventional NGCC.

| System | Performance parameter | | | |
|---|---|---|---|---|
| | Capacity | Efficiency | Cost of electricity (£/kWh) | $CO_2$ emission (kg/MWh) |
| Combined cycle gas turbine plant (CCGT) [43–45] | 634 MW | 57.4% | 0.0626 | 354 |
| Present proposed system | 225 kW | 64% | 0.18 | 311.45 |
| Natural gas fired combined cycle plant [46] | 553 MW | 55.55% | 0.07042 | 366 |

- The desirability test provides additional evidence of the analysis's accuracy. The estimated total desirability is 1. So, it is possible to say that the setting may be helpful in achieving accurate findings for every response taken individually.
- When compared to conventional Natural Gas Combined Cycle (NGCC) and Combined Cycle Gas Turbine (CCGT) power generation systems, the proposed integrated energy system offers superior thermodynamic and environmental performance.
- The system efficiency improves significantly with green hydrogen, with an estimated efficiency of 73.37%. However, the LCOE of the system is relatively high, approximately 15% higher than the methane-based option.

This study has demonstrated that the proposed power generation system can provide electricity in a more efficient and environmentally friendly way. Future implementation of this idea of the proposed plant for community-scale power production should benefit greatly from the direction provided by the current study. As a result, it can be said that the proposed power generation system can use natural gas/methane as fuel more effectively and sustainably in the long run. In terms of system thermodynamic performance, green hydrogen is more effective than methane. However, the expensive green hydrogen appears to be one of the primary impediments to its practical implementation. Future research could include an advanced exergy and exergoeconomic analyses of the proposed power generation system. Additionally, it is

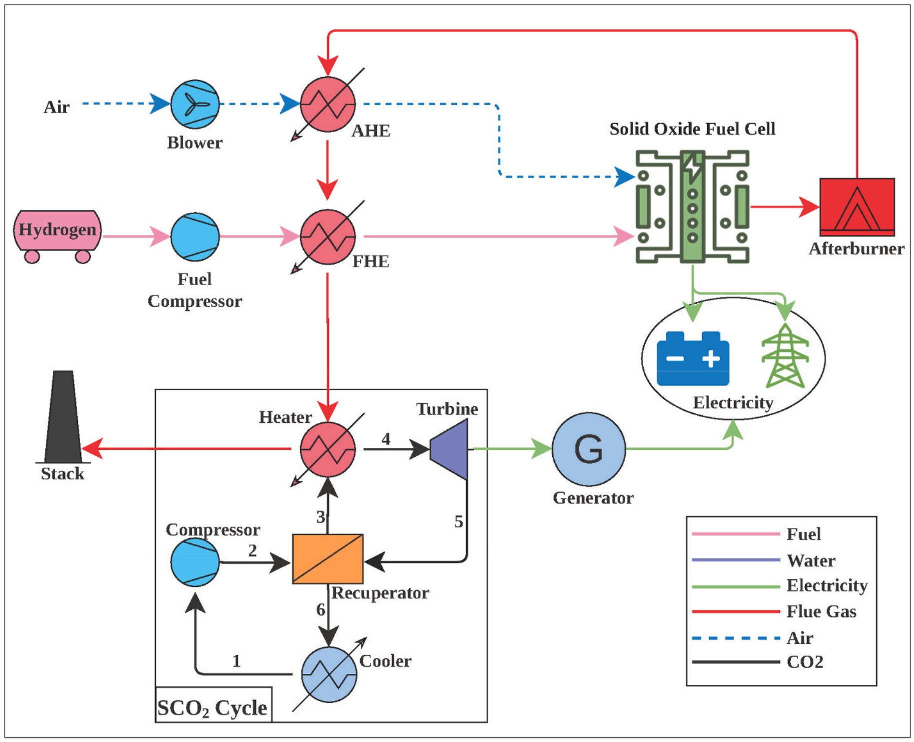


**Fig. 15.** Schematic diagram of hydrogen fuelled system.

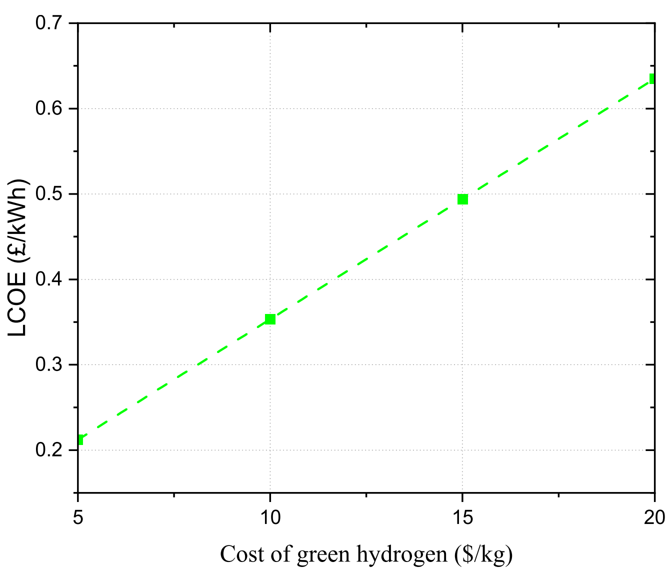


**Fig. 16.** Sensitivity analysis of LCOE with respect to cost of green hydrogen. (For interpretation of the references to colour in this figure legend, the reader is referred to the Web version of this article.)

possible to research how this proposed methane-based power generation plant can be run integrated with a Carbon Capture and Sequestration (CCS) or Carbon Capture, Utilisation and Storage (CCUS) using different types of post-combustion carbon capture systems.

## Credit author statement

Dibyendu Roy: Conceptualization, Methodology, Software, Investigation, Writing - Original Draft. Samiran Samanta: Conceptualization, Methodology, Software, Investigation, Writing - Original Draft. Sumit Roy: Conceptualization, Software, Supervision, Writing- Reviewing and Editing. Andrew Smallbone: Supervision, Project administration, Resources, Writing- Reviewing and Editing. Anthony Paul Roskilly: Supervision, Project administration, Funding acquisition.

## Declaration of competing interest

The authors declare that they have no known competing financial interests or personal relationships that could have appeared to influence the work reported in this paper.

## Data availability

Data will be made available on request.

## Acknowledgments

This research work was funded by the Engineering and Physical Science Research Council of UK (Grant number: EP/T022949/1).

## References

[1] IEA. World. Energy Outlook 2021:2021.
[2] Change IC. Mitigation of climate change. Contribution of working group III to the fifth assessment report of the intergovernmental panel on climate change 2014; 1454:147.
[3] McPhail SJ, Aarva A, Devianto H, Bove R, Moreno A. SOFC and MCFC: commonalities and opportunities for integrated research. Int J Hydrogen Energy 2011;36(16):10337–45.
[4] Marocco P, Gandiglio M, Santarelli M. When SOFC-based cogeneration systems become convenient? A cost-optimal analysis. Energy Rep 2022;8:8709–21.
[5] Roy D, Samanta S, Roy S, Smallbone A, Paul Roskilly A. Fuel cell integrated carbon negative power generation from biomass. Appl Energy 2023;331:120449.
[6] Pirkandi J, Jahromi M, Sajadi SZ, Ommian M. Thermodynamic performance analysis of three solid oxide fuel cell and gas microturbine hybrid systems for application in auxiliary power units. Clean Technol Environ Policy 2018;20(5): 1047–60.
[7] Kumar P, Choudhary T, Ansari MZ. Thermodynamic assessment of a novel SOFC and intercooled GT integration with ORC: energy and exergy analysis. Therm Sci Eng Prog 2022;34:101411.

[8] Lei Y, Ye S, Xu Y, Kong C, Xu C, Chen Y, et al. Multi-objective optimization and algorithm improvement on thermal coupling of SOFC-GT-ORC integrated system. Comput Chem Eng 2022;164:107903.
[9] Wang Z, Chen H, Xia R, Han F, Ji Y, Cai W. Energy, exergy and economy (3E) investigation of a SOFC-GT-ORC waste heat recovery system for green power ships. Therm Sci Eng Prog 2022;32:101342.
[10] Kim YS, Lee YD, Ahn KY. System integration and proof-of-concept test results of SOFC–engine hybrid power generation system. Appl Energy 2020;277:115542.
[11] Koo T, Kim YS, Lee YD, Yu S, Lee DK, Ahn KY. Exergetic evaluation of operation results of 5-kW-class SOFC-HCCI engine hybrid power generation system. Appl Energy 2021;295:117037.
[12] Mojaver P, Khalilarya S, Chitsaz A, Assadi M. Multi-objective optimization of a power generation system based SOFC using Taguchi/AHP/TOPSIS triple method. Sustain Energy Technol Assessments 2020;38:100674.
[13] Pan M, Chen X, Li X. Multi-objective analysis and optimization of cascade supercritical CO2 cycle and organic Rankine cycle systems for waste-to-energy power plant. Appl Therm Eng 2022;214:118882.
[14] Yu A, Su W, Lin X, Zhou N, Zhao L. Thermodynamic analysis on the combination of supercritical carbon dioxide power cycle and transcritical carbon dioxide refrigeration cycle for the waste heat recovery of shipboard. Energy Convers Manag 2020;221:113214.
[15] Liu Y, Wang Y, Huang D. Supercritical CO2 Brayton cycle: a state-of-the-art review. Energy 2019;189:115900.
[16] Sakalis GN. Design and partial load operation optimization of integrated ship energy system based on supercritical CO2 waste heat recovery cycle. Sustain Energy Technol Assessments 2022;51:101965.
[17] Chen H, Lu D, An J, Qiao S, Dong Y, Jiang X, et al. Thermo-Economic analysis of a novel biomass Gasification-Based power system integrated with a supercritical CO2 cycle and a Coal-Fired power plant. Energy Convers Manag 2022;266:115860.
[18] Guo J-Q, Li M-J, He Y-L, Jiang T, Ma T, Xu J-L, et al. A systematic review of supercritical carbon dioxide(S-CO2) power cycle for energy industries: technologies, key issues, and potential prospects. Energy Convers Manag 2022;258:115437.
[19] Rosa JM, Guerhardt F, Ribeiro Júnior SER, Belan PA, Lima GA, Santana JCC, et al. Modeling and optimization of reactive cotton dyeing using response surface methodology combined with artificial neural network and particle swarm techniques. Clean Technol Environ Policy 2021;23(8):2357–67.
[20] Zaman SA, Roy D, Ghosh S. Process modeling and optimization for biomass steam-gasification employing response surface methodology. Biomass Bioenergy 2020;143:105847.
[21] Sharma P, Le MP, Chhillar A, Said Z, Deepanraj B, Cao DN, et al. Using response surface methodology approach for optimizing performance and emission parameters of diesel engine powered with ternary blend of Solketal-biodiesel-diesel. Sustain Energy Technol Assessments 2022;52:102343.
[22] Ye W, Yang P, Liu Y. Multi-objective thermodynamic optimization of a free piston Stirling engine using response surface methodology. Energy Convers Manag 2018;176:147–63.
[23] Shahsavar MM, Akrami M, Gheibi M, Kavianpour B, Fathollahi-Fard AM, Behzadian K. Constructing a smart framework for supplying the biogas energy in green buildings using an integration of response surface methodology, artificial intelligence and petri net modelling. Energy Convers Manag 2021;248:114794.
[24] Guan M, Xu X, Tang X, Li Y. Optimization of supercritical CO2 extraction by response surface methodology, composition analysis and economic evaluation of bamboo green wax. J Clean Prod 2022;330:129906.
[25] Prasad KRA, John MRS. Optimization of external roller burnishing process on magnesium silicon carbide metal matrix composite using response surface methodology. J Braz Soc Mech Sci Eng 2021;43(7):342.
[26] Vidal M, Bastos D, Silva L, Gaspar D, Paulo I, Matos S, et al. Up-cycling tomato pomace by thermochemical liquefaction – a response surface methodology assessment. Biomass Bioenergy 2022;156:106324.
[27] Abbasi S, Gholamalipour A. Performance optimization of an axial turbine with a casing injection based on response surface methodology. J Braz Soc Mech Sci Eng 2021;43(9):435.
[28] Khurana H, Majumdar R, Saha SK. Response Surface Methodology-based prediction model for working fluid temperature during stand-alone operation of vertical cylindrical thermal energy storage tank. Renew Energy 2022;188:619–36.
[29] Pourali M, Esfahani JA. Performance analysis of a micro-scale integrated hydrogen production system by analytical approach, machine learning, and response surface methodology. Energy 2022;255:124553.
[30] Mojaver P, Khalilarya S, Chitsaz A. Multi-objective optimization using response surface methodology and exergy analysis of a novel integrated biomass gasification, solid oxide fuel cell and high-temperature sodium heat pipe system. Appl Therm Eng 2019;156:627–39.
[31] Ranjbar F, Chitsaz A, Mahmoudi SMS, Khalilarya S, Rosen MA. Energy and exergy assessments of a novel trigeneration system based on a solid oxide fuel cell. Energy Convers Manag 2014;87:318–27.
[32] Kim JW, Virkar AV, Fung KZ, Mehta K, Singhal SC. Polarization effects in intermediate temperature, anode-supported solid oxide fuel cells. J Electrochem Soc 1999;146(1):69–78.
[33] Chan SH, Low CF, Ding OL. Energy and exergy analysis of simple solid-oxide fuel-cell power systems. J Power Sources 2002;103(2):188–200.
[34] Rath S, Mickoleit E, Gampe U, Breitkopf C, Jäger A. Systematic analysis of additives on the performance parameters of sCO2 cycles and their individual effects on the cycle characteristics. Energy 2022;252:123957.
[35] Cigolotti V, Genovese M, Fragiacomo P. Comprehensive review on fuel cell technology for stationary applications as sustainable and efficient poly-generation energy systems. Energies 2021;14(16):4963.
[36] Industries TC. 2022.
[37] Bonalumi D, Giuffrida A, Sicali F. A case study of cascade supercritical CO2 power cycle for waste heat recovery from a small gas turbine. Energy Convers Manag X 2022;14:100212.
[38] BEIS U. Quarterly Energy Prices 2022.
[39] Palanikumar K, Davim JP. 5 - electrical discharge machining: study on machining characteristics of WC/Co composites. In: Davim JP, editor. Machining and machine-tools. Woodhead Publishing; 2013. p. 135–68.
[40] Singhal SC. Advances in solid oxide fuel cell technology. Solid State Ionics 2000;135(1):305–13.
[41] Ghodsiyeh D, Golshan A, Izman S. Multi-objective process optimization of wire electrical discharge machining based on response surface methodology. J Braz Soc Mech Sci Eng 2014;36(2):301–13.
[42] Whiston MM, Azevedo IML, Litster S, Samaras C, Whitefoot KS, Whitacre JF. Meeting U.S. Solid oxide fuel cell targets. Joule 2019;3(9):2060–5.
[43] Omehia KC, Clements AG, Michailos S, Hughes KJ, Ingham DB, Pourkashanian M. Techno-economic assessment on the fuel flexibility of a commercial scale combined cycle gas turbine integrated with a CO2 capture plant. Int J Energy Res 2020;44(11):9127–40.
[44] Rezazadeh F, Gale WF, Hughes KJ, Pourkashanian M. Performance viability of a natural gas fired combined cycle power plant integrated with post-combustion CO2 capture at part-load and temporary non-capture operations. Int J Greenh Gas Control 2015;39:397–406.
[45] Kuehn NJ, Mukherjee K, Phiambolis P, Pinkerton LL, Varghese E, Woods MC. Current and future technologies for natural gas combined cycle (NGCC) power plants. Pittsburgh, PA, Morgantown: National Energy Technology Laboratory (NETL); 2013.
[46] Hu Y, Xu G, Xu C, Yang Y. Thermodynamic analysis and techno-economic evaluation of an integrated natural gas combined cycle (NGCC) power plant with post-combustion CO2 capture. Appl Therm Eng 2017;111:308–16.
[47] Burrin D, Roy S, Roskilly AP, Smallbone A. A combined heat and green hydrogen (CHH) generator integrated with a heat network. Energy Convers Manag 2021;246:114686.
[48] Global SP. Platts hydrogen price wall. 2022.